Int. J. Heat Mass Transfer. Vol. 33, No. 1, pp. 79–90, 1990
Printed in Great Britain

0017–9310/90 $3.00 + 0.00

The effect of mixed convection instability on heat transfer in a vertical annulus

B. B. ROGERS and L. S. YAO
Department of Mechanical and Aerospace Engineering, Arizona State University, Tempe, AZ 85287, U.S.A.

(*Received* 29 *November* 1988 *and in final form* 2 *May* 1989)

Abstract—The hydrodynamic stability of mixed convection in an annulus is studied. The linear stability limit for forced flow up a vertical annulus with a constant heat flux applied to the inner wall and the outer wall insulated is determined. The result indicates that the fully-developed flow is thermally unstable in most regions of an appropriate parameter space. The magnitudes of the finite amplitude disturbances in the unstable region are determined by utilizing Stuart's shape assumption. Distorted mean flow profiles are obtained and the increase in heat transfer rates due to these disturbances are calculated from the results and agree well with the experimental data.

1. INTRODUCTION

THE STUDY of mixed convection inside ducts is a fundamental problem in heat transfer. However, the difficulties of accurately modeling the fluid motion and associated heat transfer mechanisms is often underestimated. For example, it has been demonstrated that mixed convection in vertical ducts is likely to be unstable in regions of practical interest [1–4]. In these studies the onset of instability is found to occur at relatively low heating rates. Unfortunately, many correlations for heat transfer rates in mixed convection have been obtained using simplified analyses which do not account for mixing induced by the presence of these hydrodynamic instabilities. For example, it is still common practice when modeling mixed convection to assume that the flow can be treated as steady and parallel. This assumption greatly simplifies the problem since the velocity and temperature profiles become easily predicted functions of the transverse variables only. Irrespective of the well-known theory that a velocity profile with an inflection point is a sufficient condition for inviscid instability, and that viscous flows which contain a point of inflection are usually unstable, numerical analyses utilizing the parallel flow assumption have continuously led to new 'discoveries' of physically unrealistic steady reverse flow induced by the buoyancy force. The stability analyses cited above clearly demonstrate the impossibility of the occurrence of such flows. Thus, to accurately model the fluid motion and heat transfer rates in mixed convection, mixing induced by the presence of unsteady finite amplitude disturbances must be accounted for. It is the purpose of this paper to analyze the non-linear growth of these instabilities and their subsequent effect on the heat transfer.

The increase in heat transfer rates induced by hydrodynamic instability has been observed experimentally. For example, Scheele and Hanratty [5] observed that flow in a heated vertical tube is unstable. When the buoyancy forces opposed the motion of the fluid, such as in upward flow in a cooled pipe, the transition to turbulence was abrupt. However, when the buoyancy forces aided the motion of the fluid, such as upward flow in a heated pipe, the transition to turbulence was gradual, and the initial transition resulted in a new periodic non-parallel laminar equilibrium flow. Thus, when the buoyancy forces are opposing the motion the instability is *subcritical*, and the initial flow bifurcations lead to turbulence relatively fast (in a convective time scale). In the aided flow case, however, the instability is *supercritical*, and the flow will pass through a series of equilibrium states before the transition to turbulence. The turbulence structure for such a flow is likely different than that for an isothermal flow. Flow patterns for the supercritical case in a vertical pipe were also observed by Kemeny and Somers [6] and called 'nonlaminar' to distinguish them from fully turbulent flow. Heat transfer rates were found to be as much as 30% higher then those observed in laminar flow, and the effect was observed at Reynolds numbers as small as 30. Supercritical instabilities have also been observed for heated flow in a vertical concentric annulus by Maitra and Raju [7]. In their experiment, an annulus with an inner radius to gap ratio of 0.6 was used with the inner cylinder providing a constant heat flux and the outer cylinder insulated. When the measured heat transfer rates were compared with those predicted by a model which utilized the parallel flow assumption, it was found that the observed heat transfer rates were, on average, 45% higher than predicted. In this paper, we model an annulus such as was used by Maitra and Raju so that the results can be directly compared with their experimental data.

Since the disturbance amplitudes are small near the linear stability boundary, weakly non-linear stability theory can be applied to determine the flow patterns.

NOMENCLATURE

A	curvature parameter, $b/(a-b)$
a	radius of outer cylinder
b	radius of inner cylinder
c	complex disturbance wave speed, c_r+ic_i
E	disturbance kinetic energy from radial velocity
E_w	disturbance kinetic energy from axial velocity
E_t	disturbance thermal energy
h	convective heat transfer coefficient
k	fluid thermal conductivity
Nu	Nusselt number, $h(a-b)/k$
n	azimuthal disturbance wave number
P	mean flow pressure
$\hat{P}$	disturbance pressure
Pr	Prandtl number, $\nu/\tilde{\alpha}$
Ra	Rayleigh number, $\beta g\mu(a-b)^4/\tilde{\alpha}\nu$
Re	Reynolds number, $W_{ave}(a-b)/\nu$
r	dimensional radial distance
T	upstream reference temperature
T_w	annulus inner wall temperature
t	time
t_w	time scale for wave propagation
u	radial velocity
v	azimuthal velocity
w	axial velocity
$\hat{u}$	radial disturbance velocity
$\hat{v}$	azimuthal disturbance velocity
$\hat{w}$	axial disturbance velocity
W	mean flow axial velocity
W_{ave}	average mean flow axial velocity
$\tilde{W}$	mean flow axial velocity distortion function
W_0	basic-state axial velocity
z	axial coordinate.

Greek symbols

α	axial disturbance wave number
$\tilde{\alpha}$	thermal diffusivity
β	coefficient of thermal expansion
Γ_k	amplitude of velocity disturbance
Γ_p	amplitude of pressure disturbance
Γ_t	amplitude of temperature disturbance
γ	integrals in disturbance energy balances
η	dimensionless radial coordinate, $(r-b)/(a-b)$
Θ	mean flow temperature distribution
$\tilde{\Theta}$	mean flow temperature distortion function
Θ_0	basic-state temperature distribution
θ	dimensionless temperature
$\hat{\theta}$	disturbance temperature
μ	axial wall temperature gradient
ν	kinematic viscosity
τ	time scale for disturbance growth
ϕ	azimuthal coordinate.

Stuart [8] modeled the growth of disturbances in plane-Poiseuille flow by using an integral energy approach and assuming that the disturbance retained its initial shape predicted by linear theory. This approach is often referred to as 'Stuart's shape assumption'. This method does not consider the generation of higher harmonics of the fundamental mode or the distortion of the shape of the original eigenvector, and is hence approximate [9, 10]. However, since the effect of the distortion of the disturbance is expected to be small near the neutral curve Stuart's shape assumption provides a means to determine the heat transfer rate due to extra mixing induced by instabilities and shed light on many important physical processes such as disturbance growth and energy distribution patterns.

In the modeling of the disturbance using the shape assumption, the question of the flow being subcritically or supercritically unstable becomes important. If the flow is subcritically unstable, under all but the most careful experimental conditions the flow will likely become unstable to finite amplitude disturbances before the linear stability boundary is reached, and any prediction of the structure of the flow based on the growth of the most unstable linear disturbance will probably be very much in error. However, if the instability is supercritical, the initial growth of the disturbance may be more accurately modeled by following the evolution of the linear mode than would be the case with the subcritical instability. The shape assumption utilized in this paper does not provide conclusive information about the nature of the instability. Thus, we will restrict our attention to flows which have been experimentally observed to be supercritically unstable, such as is the case in the work of Maitra and Raju.

The analysis proceeds as follows. First, a linear stability analysis is carried out to determine the stability boundary for infinitesimal disturbances and the normalized eigenfunctions of these unstable modes. These results are then used to model the shape of the distortion of the original velocity and temperature profiles due to Reynolds stresses and heat flux caused by the disturbances. At this point, the amplitude of the disturbances is not known. An integral energy balance is used to determine the equilibrium amplitudes that the disturbances will attain. The result from this analysis is used to find the distorted temperature and velocity profiles. Analysis of the modification of the heat transfer rates due to mixing induced by the unsteady flow follows from this result.

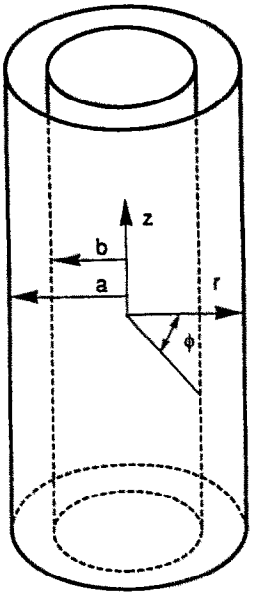

FIG. 1. Geometry and coordinates.

2. ANALYSIS

We are considering the motion of a heated fluid in a vertical concentric cylindrical annulus, the geometry of which is illustrated in Fig. 1. A constant heat flux is supplied at the inner wall and the outer wall is adiabatic. The Navier–Stokes and energy equations for incompressible flow written in terms of annular-cylindrical coordinates (r, η, z) become

$$\frac{\partial u}{\partial \eta}+\frac{u}{\eta+A}+\frac{1}{\eta+A}\frac{\partial v}{\partial \phi}+\frac{\partial w}{\partial z}=0 \tag{1a}$$

$$\frac{\partial u}{\partial t}+D_1 u-\frac{v^2}{\eta+A}=-\frac{\partial P}{\partial \eta}+\frac{1}{Re}\left[D_2^2 u-\frac{1}{(\eta+A)^2}\times\left(2\frac{\partial v}{\partial \phi}+u\right)\right] \tag{1b}$$

$$\frac{\partial v}{\partial t}+D_1 v+\frac{uv}{\eta+A}=-\frac{1}{\eta+A}\frac{\partial P}{\partial \phi}+\frac{1}{Re}\times\left[D_2^2 v+\frac{1}{(\eta+A)^2}\left(2\frac{\partial u}{\partial \phi}-v\right)\right] \tag{1c}$$

$$\frac{\partial w}{\partial t}+D_1 w=-\frac{\partial P}{\partial z}+\frac{1}{Re}[D_2^2 w]-\frac{Ra}{Re}\theta \tag{1d}$$

$$\frac{\partial \theta}{\partial t}+D_1\theta-\frac{w}{Re\,Pr}=\frac{1}{Re\,Pr}D_2^2\theta \tag{1e}$$

where

$$D_1=u\frac{\partial}{\partial \eta}+\frac{v}{\eta+A}\frac{\partial}{\partial \phi}+w\frac{\partial}{\partial z} \tag{2a}$$

and

$$D_2^2=\frac{\partial^2}{\partial \eta_2}+\frac{1}{\eta+A}\frac{\partial}{\partial \eta}+\frac{1}{(\eta+A)^2}\frac{\partial^2}{\partial \phi^2}+\frac{\partial^2}{\partial z^2}. \tag{2b}$$

In the above equations a curvature parameter of the annulus has been defined by $A=b/(a-b)$ where a and b are, respectively, the outer and inner radii of the concentric cylinders. The dimensionless radial variable is given by $\eta=(r-b)/(a-b)$. All lengths have been made dimensionless by the gap width of the annulus, $a-b$, the velocities by the mean axial velocity, W_{ave}, the pressure by ρW_{ave}^2 and the time by $(a-b)/W_{ave}$. The temperature of the inner wall is assumed to increase linearly with z as follows:

$$T_w=T_0+\mu(a-b)z.$$

A non-dimensional temperature is defined as

$$\theta=(T_w-T)(\mu(a-b)Re\,Pr).$$

In these equations, T_0 is the upstream reference temperature, T_w the wall temperature and μ the constant axial temperature gradient. The parameters in the problem are the Reynolds number $Re=W_{ave}(a-b)/\nu$, Prandtl number $Pr=\nu/\bar{\alpha}$, and the Rayleigh number $Re=\beta g\mu(a-b)^4/\bar{\alpha}\nu$, where $\bar{\alpha}$ is the coefficient of thermal diffusivity, β the thermal expansion coefficient, ν the kinematic viscosity and g the acceleration due to gravity.

We are studying the state of the fluid motion after the onset of hydrodynamic instability, when the disturbances have grown to a small but finite size. Thus, we separate the flow field into a mean flow and a disturbance (with zero mean)

$$w=W(\eta,t)+\hat{w}(\eta,\phi,z,t) \tag{3a}$$

$$u=\hat{u}(\eta,\phi,z,t) \tag{3b}$$

$$v=\hat{v}(\eta,\phi,z,t) \tag{3c}$$

$$\theta=\Theta(\eta,t)+\hat{\theta}(\eta,\phi,z,t) \tag{3d}$$

$$P=P(z,t)+\hat{P}(\eta,\phi,z,t). \tag{3e}$$

The mean flow equations are obtained by substituting these forms into the governing equations and averaging. The disturbance parameters are assumed to be represented by Fourier components in the axial and azimuthal directions and are modeled as follows:

$$\hat{\psi}=\sum_m \hat{\psi}_m(\eta,\tau)\,e^{i(\alpha(z-ct_w)+n\phi)}+\text{c.c.} \tag{4}$$

In equation (4), $\hat{\psi}$ is the disturbance quantity, α the axial wave number, n the integer azimuthal wave number, c the complex disturbance wave speed and c.c. stands for complex conjugate. Disturbances at a particular set of wave numbers will be initially amplified when the complex portion of the wave speed becomes positive. In this form two time scales are distinguished. The first time scale describes the propagation of the disturbance wave, and is given the symbol t_w, while the second represents the non-linear growth of the disturbance, and is given the symbol τ. Assuming disturbances of this nature and averaging over one wavelength with respect to axial and azimuthal coordinates, the mean-motion equations become

$$\frac{dW}{d\tau} = -\frac{dP}{dz} - \frac{Ra}{Re}\theta + \frac{1}{Re}\left[\frac{d^2W}{d\eta^2} + \frac{1}{\eta+A}\frac{dW}{d\eta}\right] - \frac{d}{d\eta}\overline{(\hat{u}\hat{w})} - \frac{\overline{\hat{u}\hat{w}}}{\eta+A} \quad (5a)$$

$$\frac{d\theta}{d\tau} = \frac{W}{Re\,Pr} + \frac{1}{Re\,Pr}\left[\frac{d^2\theta}{d\eta^2} + \frac{1}{\eta+A}\frac{\partial\theta}{\partial\eta}\right] - \frac{d}{d\eta}\overline{(\hat{u}\hat{\theta})} - \frac{\overline{\hat{u}\hat{\theta}}}{\eta+A}. \quad (5b)$$

Even though the disturbance flow patterns that we are studying in this paper are periodic and highly structured, we refer to $\overline{\hat{u}\hat{w}}$ as the averaged Reynolds stress and $\overline{\hat{u}\hat{\theta}}$ as the averaged heat flux correlation.

The mean flow equations are subject to the no-slip boundary conditions on each wall, a constant heat flux applied at the inner wall and an insulated outer wall. With our scaling, the boundary conditions become

$$W(0) = W(1) = \Theta(0) = \Theta'(1) = 0. \quad (6)$$

Subtracting the mean flow equations (5) from the governing equations (1) we arrive at the relations describing the disturbance

$$\frac{\partial\hat{u}}{\partial\eta} + \frac{\hat{u}}{\eta+A} + \frac{1}{\eta+A}\frac{\partial\hat{v}}{\partial\phi} + \frac{\partial\hat{w}}{\partial z} = 0 \quad (7a)$$

$$\frac{\partial\hat{u}}{\partial t} + W\frac{\partial\hat{u}}{\partial z} + D_1\hat{u} - \frac{\hat{v}^2}{\eta+A} = -\frac{\partial\hat{P}}{\partial\eta} + \frac{1}{Re}\times\left[D_2^2\hat{u} - \frac{1}{(\eta+A)^2}\left(2\frac{\partial\hat{v}}{\partial\phi} + \hat{u}\right)\right] \quad (7b)$$

$$\frac{\partial\hat{v}}{\partial t} + W\frac{\partial\hat{v}}{\partial z} + D_1\hat{v} + \frac{\hat{u}\hat{v}}{\eta+A} = -\frac{1}{\eta+A}\frac{\partial\hat{P}}{\partial\phi} + \frac{1}{Re}\times\left[D_2^2\hat{v} + \frac{1}{(\eta+A)^2}\left(2\frac{\partial\hat{u}}{\partial\phi} - \hat{v}\right)\right] \quad (7c)$$

$$\frac{\partial\hat{w}}{\partial t} + \hat{u} + W\frac{\partial\hat{w}}{\partial z} + D_1\hat{w} = -\frac{\partial\hat{P}}{\partial z} + \frac{1}{Re}[D_2^2\hat{w}] - \frac{Ra}{Re}\hat{\theta} \quad (7d)$$

$$\frac{\partial\hat{\theta}}{\partial t} + \hat{u}\frac{\partial\Theta}{\partial\eta} + W\frac{\partial\hat{\theta}}{\partial z} D_1\hat{\theta} - \frac{\hat{w}}{Re\,Pr} = \frac{1}{Re\,Pr}D_2^2\hat{\theta}. \quad (7e)$$

In these equations D_1 differs slightly from the form given by equation (2a) in that the velocities are disturbance velocities. Because of these convective terms, the equations are nonlinear in the disturbance parameters.

3. THE LINEAR STABILITY SOLUTION

The solution of the linear stability problem for mixed convection is described in detail in refs. [1–4]. Briefly, the procedure goes as follows. The basic-state velocity and temperature profiles are found by assuming the flow is steady, laminar, fully developed and parallel. Results for the basic-state calculation for a curvature parameter of 0.6 are shown in Fig. 2. The linear stability equations are obtained from equations (7) by neglecting the small non-linear terms. The resulting set of partial differential equations are converted to ordinary differential equations by the assumption of the normal mode form for the disturbances, as given by equation (4), with only the first harmonic term in the series being considered. The resulting set of five linear equations is then reduced to three through the elimination of the pressure terms by cross-differentiation, and the choice of appropriate streamfunctions to satisfy the continuity equation. The ensuing equations, along with the no-slip boundary conditions for each disturbance quantity applied at the walls, form a complex eigenvalue problem for the disturbance wave speed, c, with the disturbance being unstable for $c_i > 0$. Thus, at a given Pr, the stability boundary is determined to be that locus of points in the (Ra, Re, α, n) space where $c_i = 0$. These points are found by a numerical search. The numerical techniques used in the analysis are described in detail in refs. [1–4].

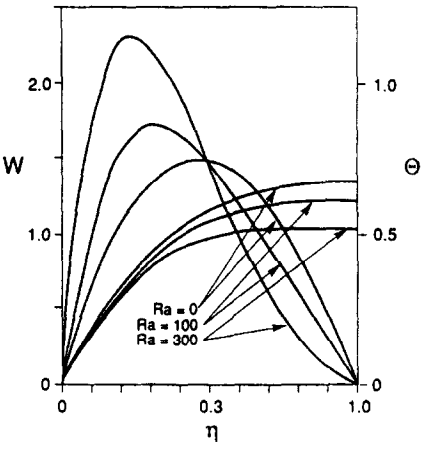

FIG. 2. Basic-state velocity and temperature profiles for $A = 0.6$.

The instability boundary for $A = 0.6$ and $Pr = 6$ in the (Ra, Re) plane is shown in Fig. 3. The result indicates that at $Re > 100$ the instability boundary is a very weak function of Re and the flow becomes unstable to a thermal instability at about $Ra = 89$. At $Re < 50$, the inertial forces are minimal and the critical Ra increases. The azimuthal wave number for this instability is $n = 0$, hence the most unstable disturbance is axisymmetric. This curve is similar in shape to that presented in ref. [1] for upward flow in a heated vertical pipe, and reaffirms the assertion that mixed convection flows become unstable even at quite small heating rates with rather minimal distortion of the velocity profile. For example, in this geometry a point of inflection does not appear in the basic-state velocity profile until $Ra = 96$, which is already in the unstable region (see Fig. 2). The range of data presented by Maitra and Raju occurs between Re of about 150 and 500 and at Ra between about 200 and

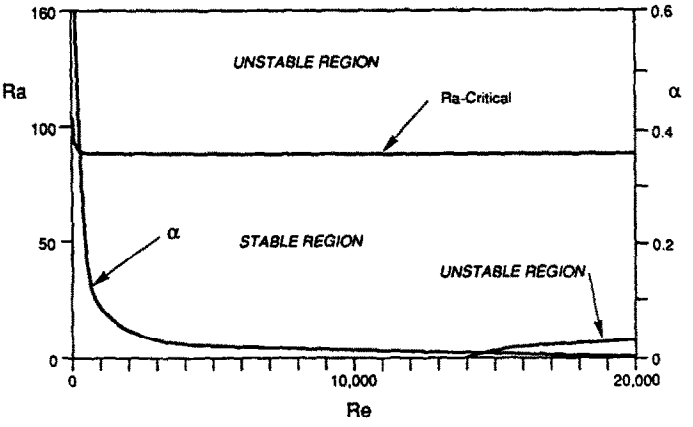

FIG. 3. Linear stability boundary and axial wave number vs Ra for $Pr = 6$ and $A = 0.6$.

10 000. Thus, their experimental data were taken well into the unstable region and the observed increase in heat transfer rates is not surprising.

A shear instability occurs when isothermal flow in the annulus becomes unstable to a non-axisymmetric disturbance, with an azimuthal wave number of $n = 1$, at a Reynolds number of about 14 000, in agreement with ref. [11]. With small amounts of heat addition we find that this instability is stabilized, and the shape of the stability boundary becomes almost parallel to the horizontal axis at a Rayleigh number of about 8. The stable region then consists of a region below the thermal instability, which occurs at a Rayleigh number of about 89, and above the shear instability, which is unstable below Rayleigh numbers of about 8. A search to $Re = 50\,000$ was unsuccessful in locating additional instabilities which would bridge this gap. The thermal and shear instability curves are not quite horizontal, however, and extrapolation of these curves indicates that they may intersect at large Reynolds numbers. This behavior is similar to that reported in refs. [3, 4], but in those cases an interactive instability was found which bridged the gap from the thermal to shear instabilities. It is known that isothermal channel flows become unstable to finite amplitude disturbances at Reynolds numbers of a few thousand. Thus, the shear instability found here will be of the subcritical type.

A plot of axial wave number vs Re for the thermal instability is also given on Fig. 3, and illustrates that the wave number, α, decreases with increasing Re. As Re doubles (corresponding to a doubling of the mean axial velocity), α decreases by about half. This indicates a lengthening of the disturbance with increasing mean flow.

It is found that, in this case, the thermal disturbance wave speed, c_r, is almost constant with Re at a non-dimensional value of 1.65. This speed is slightly slower than the maximum axial velocity, but faster than the mean velocity. Thus, there will be two critical layers in the velocity profile. At $Ra = 89$ these occur at about $\eta = 0.23$ and 0.41.

4. THE FINITE-AMPLITUDE SOLUTION

4.1. *Mean flow*

Through the action of the Reynolds stress and heat flux terms, the mean flow, given by equations (5), will begin to differ from the basic state as the disturbance grows. In the case of a supercritical instability, such as has been observed in this situation, the disturbance will grow until it reaches an equilibrium amplitude. Since we are interested in finding this amplitude, we obtain the equilibrium solution to the mean flow equations by setting the time derivatives to zero. This is analogous to the 'method of false problems' described by Reynolds and Potter [12]. In addition, we will impose the requirement that the mean mass-flow rate through the channel remain constant. Thus, the pressure gradient driving the flow must be adjusted to account for the variation in wall shear stress as the disturbance distorts the mean motion.

In general, we must allow separate amplitudes for the velocity and thermal disturbances. Investigation of the mean flow equations reveals the Reynolds stress and heat flux terms are of the order of amplitude squared, and we thus expect the distortion of the basic state to also be of this order. Thus, we model the mean flow as the basic state plus a distortion of the basic state as follows:

$$W = W_0 + \Gamma_k^2 \tilde{W} \tag{8a}$$

$$\Theta = \Theta_0 + \Gamma_t \Gamma_k \tilde{\Theta} \tag{8b}$$

where Γ_k and Γ_t are the amplitudes of the velocity and temperature disturbances, respectively, W_0 and Θ_0 the basic state, and $\tilde{W}$ and $\tilde{\Theta}$ represent the distortion of the mean flow from the basic state.

The equations for the mean distortion quantities which result at the order of the amplitude squared are solved using the results from the linear analysis to model the Reynolds stress and heat flux terms. Since the amplitudes are initially unknown and the ratio of the amplitudes will appear in the mean flow distortion equations, the system must be solved in an iterative

fashion simultaneously with the solution for the amplitudes.

4.2. *Disturbance*

The results from the linear stability calculation for the situation being considered in this study shows that the most unstable disturbance is axisymmetric. Thus, the azimuthal disturbance velocity is zero and the azimuthal momentum equation is not necessary. If we multiply each disturbance equation by its primary variable and integrate over one wavelength of the disturbance we obtain, for the axisymmetric case, the following integral relations for the conservation of kinetic and thermal energy:

$$\frac{dE_w}{dt} = \gamma_{wu} + \gamma_{wp1} + \gamma_{wp2} + \gamma_{w\theta} + \gamma_{wd} \tag{9a}$$

$$\frac{dE_u}{dt} = \gamma_{uw} + \gamma_{ud} \tag{9b}$$

$$\frac{dE_t}{dt} = \gamma_{\theta p1} + \gamma_{\theta p2} + \gamma_{\theta w} + \gamma_{\theta d} \tag{9c}$$

where E_w is the kinetic energy from the axial component of the disturbance velocity contained within the disturbance volume, E_u the kinetic energy from the radial disturbance velocity and E_t is identified as a total disturbance thermal energy within the volume. The term 'thermal energy' is used in this case to describe the integral over the volume of the disturbance temperature squared. The expressions for the γ's are

$$\gamma_{wu} = \Gamma_k \Gamma_p \int_0^1 \overline{\hat{P}\frac{\partial \hat{w}}{\partial z}}(\eta + A)\, d\eta \tag{10a}$$

$$\gamma_{wp1} = -\Gamma_k^2 \int_0^1 \overline{(\hat{u}\hat{w})}\frac{dW_0}{d\eta}(\eta + A)\, d\eta \tag{10b}$$

$$\gamma_{wp2} = -\Gamma_k^4 \int_0^1 \overline{(\hat{u}\hat{w})}\frac{d\tilde{W}}{d\eta}(\eta + A)\, d\eta \tag{10c}$$

$$\gamma_{w\theta} = -\Gamma_k \Gamma_t \int_0^1 \overline{(\hat{w}\hat{\theta})}\frac{Ra}{Re}(\eta + A)\, d\eta \tag{10d}$$

$$\gamma_{wd} = \frac{\Gamma_k^2}{Re}\int_0^1 [\hat{w}D_2^2\hat{w}](\eta + A)\, d\eta \tag{10e}$$

$$\gamma_{uw} = \Gamma_k \Gamma_p \int_0^1 \overline{\hat{P}\left[\frac{\partial \hat{u}}{\partial \eta} + \frac{\hat{u}}{(\eta + A)}\right]}(\eta + A)\, d\eta \tag{10f}$$

$$\gamma_{ud} = \frac{\Gamma_k^2}{Re}\int_0^1 \left[\overline{\hat{u}D_2^2\hat{u}} - \frac{\overline{\hat{u}^2}}{(\eta + A)^2}\right](\eta + A)\, d\eta \tag{10g}$$

$$\gamma_{\theta p1} = -\Gamma_k \Gamma_t \int_0^1 \overline{(\hat{u}\hat{\theta})}\frac{d\Theta_0}{d\eta}(\eta + A)\, d\eta \tag{10h}$$

$$\gamma_{\theta p2} = -\Gamma_k^2 \Gamma_t^2 \int_0^1 \overline{(\hat{u}\hat{\theta})}\frac{d\tilde{\Theta}}{d\eta}(\eta + A)\, d\eta \tag{10i}$$

$$\gamma_{\theta w} = \Gamma_k \Gamma_t \int_0^1 \frac{\overline{\hat{w}\hat{\theta}}}{Re\, Pr}(\eta + A)\, d\eta \tag{10j}$$

$$\gamma_{\theta d} = \frac{\Gamma_t^2}{Re\, Pr}\int_0^1 [\hat{\theta}D_2^2\hat{\theta}](\eta + A)\, d\eta \tag{10k}$$

where the term Γ_p in equations (10a) and (10f) represents the amplitude of the pressure disturbance, and the overbars in equations (10) mean that the quantities have been averaged over the wavelength of a disturbance. The disturbance quantities in these integrals represent the $O(1)$ result from the linear stability problem multiplied by the appropriate disturbance amplitude. If we consider the equilibrium solution, the time-dependent terms on the left-hand side of equations (9) go to zero, and we are left with steady-state energy balances for the thermal and kinetic disturbance energies.

The pressure scrambling term in equation (9a), γ_{wu}, represents the redistribution of disturbance kinetic energy from the axial velocity component to the radial velocity component. Since there is no mean flow in the radial direction there is no direct radial disturbance energy production and this term will be the only source of radial kinetic energy. Its value will be negative since the radial kinetic energy is gained at the expense of the axial kinetic energy. The second term in this equation, γ_{wp1}, represents the production of the axial disturbance kinetic energy by the action of the Reynolds stress and mean flow strain, and is positive. The third term, γ_{wp2}, represents the modification of the axial kinetic energy production due to the distortion of the mean flow, and is negative. The fourth term, $\gamma_{w\theta}$, represents the exchange between the thermal disturbance energy and the axial disturbance kinetic energy through the buoyant force. The last term, γ_{wd}, represents the dissipation of the axial disturbance kinetic energy through viscous action, and is always negative. The first term in equation (9b), γ_{uw}, represents the transfer of disturbance kinetic energy between the axial and radial components of the disturbance kinetic energy. This term will be equal in magnitude, but opposite in sign to γ_{wu}. The other term in equation (9b), γ_{ud}, accounts for the viscous dissipation of radial disturbance kinetic energy. The first term in equation (9c), $\gamma_{\theta p1}$, represents the production of disturbance thermal energy from the mean temperature gradient, and is positive. The second term, $\gamma_{\theta p2}$, represents a correction to $\gamma_{\theta p1}$ due to the distortion of the mean temperature gradient, and is negative. The third term in this equation, $\gamma_{\theta w}$, represents the transfer of disturbance thermal energy to axial disturbance kinetic energy through the buoyant force. The last term in this equation, $\gamma_{\theta d}$, represents the thermal disturbance energy dissipated by conduction, and is negative. The thermal/kinetic energy exchange terms in equations (9a) and (9c) represents a redistribution of the disturbance energy between the thermal and kinetic energy components of the total

disturbance energy. This interaction represents the key energy transfer mechanism in mixed-convection instability.

The terms in the energy balances given by equations (9) describe the energy transfer patterns between the mean motion and the disturbance, as well as among the various disturbance energy components. The total disturbance energy is produced by the mean temperature gradient, which produces the thermal energy, and by the Reynolds stress/mean flow strain interaction which produces axial disturbance kinetic energy. Another source of axial kinetic energy is the exchange of disturbance energy from the thermal to kinetic energy components of the total disturbance energy through the buoyant force. These kinetic energy production terms are in competition with the dissipation and energy redistribution terms in the axial momentum equation. Some of the axial disturbance kinetic energy will be dissipated by the axial viscous dissipation term. Additional energy will be transferred from the axial to radial components of the kinetic energy through the disturbance pressure fluctuations, where it is dissipated by viscous action in the radial direction. The thermal disturbance energy that is not transferred to the disturbance kinetic energy through the bouyant force will be dissipated by conduction. When production and dissipation rates are equivalent, a steady state will result.

The determination of the amplitudes from equations (9) and (10) is straightforward. Briefly, the procedure is as follows. First, by combining equations (9a) and (9b), the pressure is eliminated from the integral energy balances. This results in a set of two equations, the first being a balance of the total disturbance kinetic energy and the second being the thermal energy balance. The integrals in these energy balances are evaluated using results from the solution of the linear stability problem. The resulting equations then represent an easily solved system of two equations for the two unknown amplitudes, Γ_k and Γ_t. As mentioned earlier, however, the solution for the amplitudes will require an iterative procedure since the amplitude ratio appears in the mean flow distortion equations. After the determination of the kinetic energy and thermal disturbance amplitudes, the pressure disturbance amplitude is easily found from equation (9b).

4.3. *Disturbance amplitudes*

The linear stability results show that the critical *Ra* is only a very weak function of *Re*. The velocity and temperature profiles for the basic state are functions of *Ra* only, hence the disturbance initially perturbs velocity and temperature profiles which are very similar throughout the range of *Re* considered. The amplitudes of the disturbances are determined from the energy balances given by equations (9). From equations (9a) and (10e), we see that an increase in *Re* will lead to a decrease in the viscous dissipation term. However, the thermal/kinetic energy exchange term also includes *Re* in the denominator, and hence will decrease by a proportional amount. In addition, in this particular case a doubling of *Re* leads to a doubling of the critical disturbance wavelength, and the radial velocity will decrease in an amount proportional to the increase in *Re*. Hence, the amplitude of this disturbance at a given *Ra* is dependent only on the mean velocity and temperature profiles and the critical *Ra*. Since these quantities are not strong functions of *Re*, our model predicts almost no dependence on the Reynolds number, and our results will be presented at a single value of *Re*. It should be understood, however, that this behavior is due to the nature of the instability, and is not expected to be the general case for all curvature parameters and Prandtl numbers.

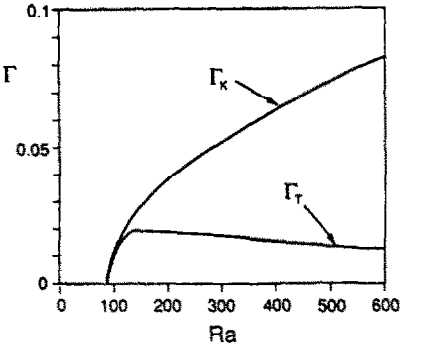

FIG. 4. Disturbance amplitudes for velocity and temperature disturbances: Γ_k, velocity disturbance; Γ_t, temperature disturbance.

Figure 4 illustrates the kinetic and thermal energy amplitudes as functions of *Ra* for $Re = 250$. The magnitudes of the amplitudes shown in this figure are referenced to the magnitude of the eigenmodes for the disturbance velocities and temperatures and hence depend on the normalization used for these vectors. In this paper, the following normalizations were used:

$$\text{velocities:} \quad v_n^2 = \tfrac{1}{2}\int_0^1 (u^2+w^2)\,\mathrm{d}\eta$$

$$\text{temperature:} \quad \theta_n^2 = \tfrac{1}{2}\int_0^1 (\theta^2)\,\mathrm{d}\eta.$$

From Fig. 4 we see that the momentum disturbance amplitude increases continuously with increasing *Ra*. The thermal disturbance amplitude, however, increases to a maximum value at about $Ra = 150$, then begins to decrease. This occurs for two reasons. First, disturbance thermal energy is being converted to kinetic energy through the disturbance energy exchange mechanism discussed earlier. Second, the production of thermal disturbance energy through the Reynolds heat flux term is decreasing in magnitude. This is because the mean temperature profile is flattening out due to the presence of the disturbance, and hence the mean temperature gradient, which drives the production of the thermal disturbance energy, is decreasing.

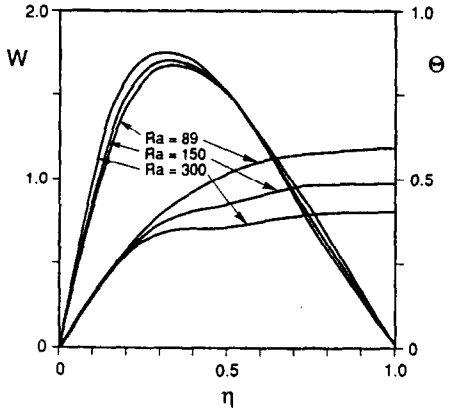

FIG. 5. Distorted mean velocity and temperature profiles.

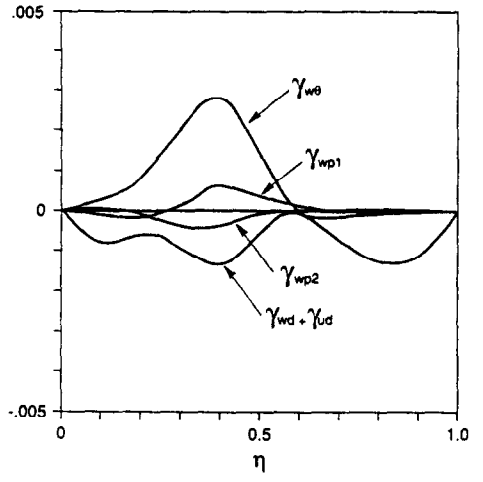

FIG. 6. Integrands in disturbance kinetic energy balance at $Ra = 150$.

Plots of the distorted mean velocity and temperature profiles for $Re = 250$ and several Ra are shown in Fig. 5. This figure illustrates that the velocity profile is enhanced near the inner wall and slightly retarded near the outer wall as Ra increases. This occurs because the buoyant force in the mean flow equations acts in the axial direction and tends to increase the flow rate. This effect is greatest near the heated inner wall and least near the insulated outer wall. Because of the requirement of mass conservation, the velocity near the outer wall must decrease to make up for the increase near the inner wall. This effect is similar to that obtained from the parallel flow assumption, but comparison of Figs. 2 and 5 illustrates that the cross stream exchange of momentum due to the disturbance minimizes this effect for the distorted flow.

The distorted mean temperature profiles shown on Fig. 5 clearly illustrate the enhancement in heat transfer due to the presence of the disturbance. We see that the temperature difference between the inner and outer walls decreases significantly as Ra increases. Comparison of these results with those obtained from the parallel flow assumption, as shown in Fig. 2, shows that this decrease is a great deal larger due to the presence of the disturbance. The temperature gradient at the inner wall is not affected significantly. Thus, the same amount of heat is being transferred into the duct with a much smaller difference between the inner wall temperature and the fluid mixed-mean temperature.

4.4. *Energetics*

An explanation of many of the phenomena observed in these results requires a more detailed study of the energy balances. Figures 6 and 7 are plots of the integrands in equations (9) vs the radial coordinate at $Re = 250$ and $Ra = 150$. The results on Fig. 6 are for the total kinetic energy balance, involving both radial and axial velocities, while those on Fig. 7 refer to the thermal energy balance. We see from Fig. 6 that the kinetic energy production term, γ_{wp1}, is positive. It is dominated, however, by the production of kinetic energy through exchange of disturbance energy with the thermal component of the total disturbance energy. Both production terms reach their maximum values near the outer critical layer at $\eta = 0.41$. However, the energy exchange term, $\gamma_{w\theta}$, reaches a maximum amplitude approximately four times as large as the shear production term, γ_{wp1}. The mean flow distortion term, γ_{wp2}, is negative and also reaches its minimum value near the outer critical layer. The viscous dissipation term, $\gamma_{wd}+\gamma_{ud}$, is negative, as expected. The plot of this term reveals that the viscous dissipation is largest near the outer critical layer, and also has maxima in the regions of high shear rates.

In Fig. 7, we see that the production of disturbance thermal energy through the Reynolds heat flux term, $\gamma_{\theta p1}$, is positive throughout the domain and reaches its maximum value near the outer critical layer. The mean temperature distortion term, $\gamma_{\theta p2}$, is negative throughout most of the domain. The energy exchange term, given by $\gamma_{\theta w}$, is negative as expected. Its magnitude, however, is a great deal smaller than the magnitude of the other terms in the thermal energy balance. Thus, although it is the dominant term in the kinetic energy balance, it does not significantly reduce

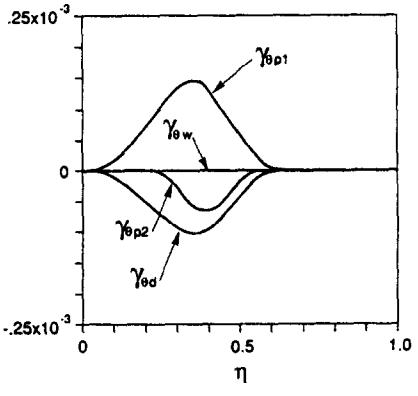

FIG. 7. Integrands in disturbance thermal energy balance at $Ra = 150$.

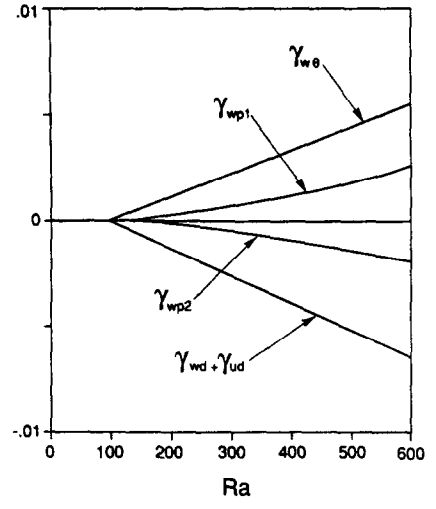

FIG. 8. Integrals in disturbance kinetic energy balance vs *Ra*.

the production of thermal energy. The dissipation of thermal energy due to conduction, given by $\gamma_{\theta d}$, is seen to be negative throughout the domain. All of the terms shown on this plot become very small by about $\eta = 0.6$. Thus, the temperature profiles will not be affected by the disturbance near the outer wall, but the profiles will be modified significantly in the regions near the critical layer. This is illustrated in Fig. 5, which shows the mean distorted temperature profiles as discussed earlier. In this figure we see that the profiles are quite different near the channel center, but become similar at the walls.

The values of the terms in the energy balances, equations (9), are plotted vs *Ra*, at $Re = 250$, in Figs. 8 and 9 for the total kinetic and thermal energy respectively. In Fig. 8 we see that the thermal/kinetic energy exchange term, $\gamma_{w\theta}$, is the dominant kinetic energy production term throughout the range of *Ra* investigated. However, as *Ra* increases, the relative importance of the shear flow production term, γ_{wp1}, increases.

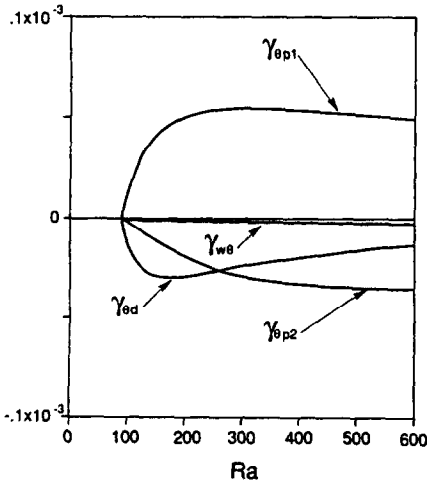

FIG. 9. Integrals in disturbance thermal energy balance vs *Ra*.

This is a consequence of the shape assumption, and occurs because the energy exchange term, $\gamma_{w\theta}$, increases linearly with *Ra* and is multiplied by the amplitude of the thermal disturbance, Γ_t, and the amplitude of the kinetic energy disturbance, Γ_k. The shear flow production term, however, is multiplied by Γ_k^2. Since the amplitude of the thermal disturbance begins to decrease after about $Ra = 150$, the rate of increase of the energy exchange term with increasing *Ra* will be smaller beyond this point. The kinetic energy amplitude continues to increase, however, and hence this term begins to increase faster with increasing *Ra*. Figure 8 also illustrates that the mean flow distortion term, γ_{wp2}, decreases with increasing *Ra*, as does the viscous dissipation term, $\gamma_{wd}+\gamma_{ud}$, thus balancing the production terms. The mean flow distortion term is close to a mirror image of the shear flow production term and the viscous dissipation closely mirrors the energy exchange term.

Figure 9 illustrates the magnitudes of the terms in the thermal energy balance as *Ra* increases. We see from this figure that the thermal energy production term, $\gamma_{\theta p1}$, initially increases with increasing *Ra*, but begins to decrease at Rayleigh numbers larger than about 250. As discussed earlier, this is due to the fact that the temperature profile is flattening out, hence the driving gradient in the thermal energy production term is decreasing. We also see that the energy exchange term, $\gamma_{\theta w}$, is negative, indicating that thermal energy is being converted into kinetic energy as observed earlier. In this case, however, we see that the magnitude of this term is small in comparison to the magnitude of the other terms in the thermal energy balance. Thus, the reduction in the amplitude of the thermal disturbance is due primarily to the reduction in the production term. Figure 9 also illustrates that the thermal energy dissipation due to conduction initially increases, but then begins to decrease as the amplitude of the thermal energy disturbance decreases. This, again, is a consequence of the shape assumption model for the disturbance. Since the shape of the disturbance is assumed to not change, the energy dissipation integral will remain constant with changing *Ra*. This integral is multiplied by the square of the thermal energy disturbance amplitude and, if the amplitude decreases, the dissipation will likewise decrease. The magnitude of the mean temperature distortion term, $\gamma_{\theta p2}$, increases with increasing *Ra*. As the magnitude of the dissipation decreases at larger *Ra*, we see that it becomes a dominant term. Thus we notice rather large distortions of the mean temperature profile at higher *Ra*, as seen in Fig. 5.

4.5. *Disturbance shape*

A plot of the periodic temperature disturbance in convective coordinates is given in Fig. 10. This figure illustrates that the temperature profile will be perturbed the greatest amount in the region of the outer critical layer, and the value of the disturbance becomes very small by about $\eta = 0.8$. This is reflected in Fig.

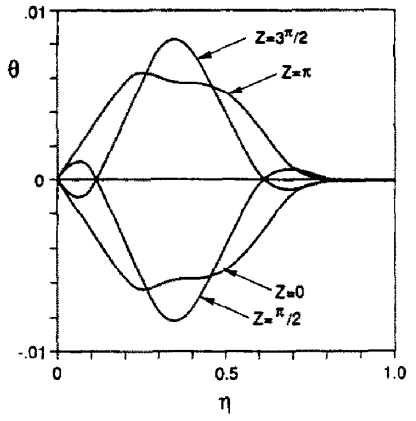

FIG. 10. Temperature disturbance in convective coordinates ($Z = \alpha(z-ct)$).

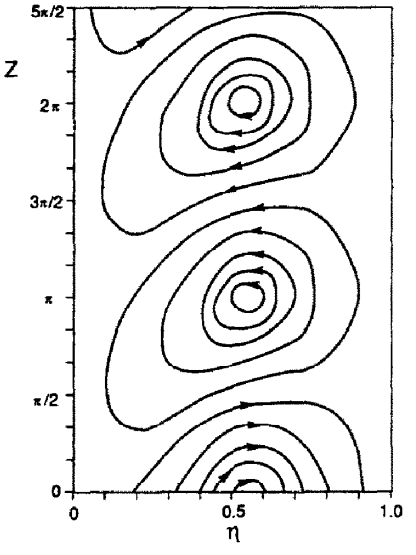

FIG. 11. Disturbance streamlines in convective coordinates ($Z = \alpha(z-ct)$).

5, which shows the temperature wave has very little effect on the mean temperature profile near the outer wall, but in the region around the critical layer the shape of the profile differs a great deal from that predicted by the parallel flow assumption.

Figure 11 is a plot of the velocity disturbance streamlines in convective coordinates. The figure illustrates that the disturbance will consist of a set of counter-rotating cells, tilted slightly upward toward the outer wall. The vertical axis on this plot is the convective coordinate, $Z = \alpha(z-ct)$, and is not to scale. The critical axial wave number, α, at $Re = 250$ is 0.26, corresponding to a disturbance wavelength that is about 25 times the annular gap-width. Hence, the disturbance radial velocities, as well as the amplitudes of the pressure fluctuations, will be quite small in comparison to the axial disturbance velocities.

5. HEAT TRANSFER AND FRICTION COEFFICIENT

The effect of the distortion of the mean velocity and temperature profiles on the heat transfer rate is studied by defining a Nusselt modulus as follows:

$$Nu = \frac{h(a-b)}{k}.$$

In this equation, h is the convective heat transfer coefficient based on the temperature difference between the inner wall of the annulus and the fluid mixed-mean temperature, and k the thermal conductivity of the fluid. This Nusselt number can also be written as

$$Nu = \frac{\int_0^1 W(\eta+A)\,d\eta}{\int_0^1 W\Theta(\eta+A)\,d\eta}\left.\frac{\partial\Theta}{\partial\eta}\right|_{\eta=0}. \tag{11}$$

After the distorted mean velocity and temperature profiles have been determined, the Nusselt number is found from equation (11). Results of this calculation, as well as results from the parallel flow assumption, for $Re = 250$ are illustrated in Fig. 12. The range of experimental data from Maitra and Raju is also illustrated on this plot. This figure clearly demonstrates that mixing increases heat transfer rates above those predicted by the parallel flow assumption. At $Ra = 100$, the increase in Nu is found to be about 5%, and at $Ra = 200$, this has increased to 20%. The data presented by Maitra and Raju starts at Ra of about 200, as illustrated in the figure. At this Ra, our result is near the center of the experimental data. However, as Ra increases our predictions fall out of the range of data. This is not surprising, however, since this analysis can be expected to be more accurate near the neutral curve. At larger values of Ra the fluid will undergo subsequent bifurcations which will lead to stronger mixing, and this increased mixing will cause the observed increase in Nu to be larger than predicted. An analysis of these effects at larger values of Ra will likely require a solution of the fully non-linear governing equations. However, these results clearly demonstrate that the observed increase in Nu is due to the presence of hydrodynamic instabilities and any attempt to model the heat transfer rates in mixed convection which does not account for the presence of these disturbances will be very much in error.

In the region between the linear stability limit and $Ra = 600$, our analytical result for the Nusselt number of the distorted flow, as shown on Fig. 12, is described closely by the following relation between Ra and Nu:

$$Nu = 1.02\,(Ra)^{0.28}. \tag{12}$$

As mentioned previously, the dependence of the distorted velocity and temperature on Re is found to be minimal. Thus, since the Nusselt number is obtained from these profiles, it will also not have a strong dependence on Re. It can be expected that the flow in an annulus will become fully turbulent due to

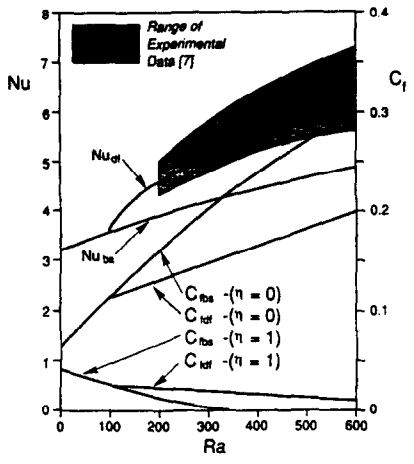

FIG. 12. Nusselt number and wall shear stress vs Rayleigh number at $Re = 250$. The subscript 'bs' stands for basic state, while the subscript 'df' stands for distorted flow.

a subcritical shear instability at a Reynolds number of a few thousand. Hence, the correlation given by equation (12) can be expected to provide results similar to those shown in Fig. 12 throughout the range of *Re* which provide laminar isothermal flow in an annulus of this curvature parameter.

The dimensionless shear stress, or friction coefficient, at each wall is also plotted in Fig. 12 for both the disturbed flow and the basic state. Since the disturbance flattens out the velocity profile we see that the magnitude of the shear stress on the inner wall increases much slower in the disturbed flow than is predicted by the parallel flow assumption. At an *Ra* of about 350, the shear stress on the outer wall predicted by the basic state goes to zero, corresponding to 'flow reversal'. This figure clearly illustrates that this event will not occur, since the shear stress does not go to zero for the disturbed flow. In addition, at higher values of *Ra* the flow will undergo subsequent bifurcations which will increase the value of the outer wall shear stress beyond that predicted by this analysis.

6. CONCLUSIONS

The marginal stability boundary from linear theory has been determined for mixed convection flow up a vertical annulus with an inner radius to gap ratio of 0.6, a constant heat flux applied to the inner cylinder, the outer cylinder being insulated. These results compliment those obtained in earlier studies [1–4], and reaffirm the observation that mixed convection flows in ducts are unstable over a very large portion of the parameter domain. These instabilities occur at heating rates a great deal smaller than those necessary to produce 'reverse flow' regions predicted by models utilizing the parallel flow assumption.

The effect of non-linear disturbance growth is modeled by obtaining estimates for disturbance amplitudes with the aid of disturbance energy balances and Stuart's shape assumption. Study of the energy balances for the thermal and kinetic disturbance energies shows that the primary source of production of disturbance kinetic energy is not through direct production from the shear flow, but rather through exchange of energy with the thermal disturbance. While this energy exchange is a dominant term in the kinetic energy balance, its effect on the production of thermal disturbance energy is small.

The results obtained from this analysis predict Nusselt numbers that fall within the range of experimental data for Rayleigh numbers that are not much larger than the critical Rayleigh number. This clearly indicates that the observed increases in heat transfer rates beyond those predicted by parallel flow analyses can be attributed to the presence of hydrodynamic instabilities. Consequently, efforts to accurately model the velocity and temperature fields must consider the presence of mixing induced by these disturbances. Heat transfer correlations developed from analytical models which utilize the parallel flow assumption will be valid only at very low heat addition rates and must therefore be used with extreme caution. Accurate modeling of these phenomena at *Ra* a large distance from the neutral curve will probably require a solution of the fully non-linear governing equations.

REFERENCES

1. L. S. Yao, Is fully-developed and non-isothermal flow possible in a vertical pipe? *Int. J. Heat Mass Transfer* **30**, 707–716 (1987).
2. L. S. Yao, Linear stability analysis for opposing mixed convection in a vertical pipe, *Int. J. Heat Mass Transfer* **30**, 810–811 (1987).
3. L. S. Yao and B. B. Rogers, The linear stability of mixed convection in a vertical annulus, *J. Fluid Mech.* **201**, 279–298 (1989).
4. L. S. Yao and B. B. Rogers, Mixed convection in an annulus of large aspect ratio, *J. Heat Transfer* **111**(3), 683–689 (1989).
5. G. F. Scheele and T. J. Hanratty, Effect of natural convection on stability of flow in a vertical pipe, *J. Fluid Mech.* **14**, 244–256 (1962).
6. G. A. Kemeny and E. V. Somers, Combined free and forced convective flow in vertical circular tubes—experiments with water and oil, *J. Heat Transfer* **84**, 339–346 (1962).
7. D. Maitra and K. S. Raju, Combined free and forced convection laminar heat transfer in a vertical annulus, *J. Heat Transfer* **97**, 135–137 (1975).
8. J. T. Stuart, On the non-linear mechanics of hydrodynamic instability, *J. Fluid Mech.* **4**, 1–21 (1958).
9. J. T. Stuart, On the non-linear mechanics of wave disturbances in stable and unstable parallel flows—Part 1. The basic behavior in plane-Poiseuille flow, *J. Fluid Mech.* **9**, 353–370 (1960).
10. J. Watson, On the non-linear mechanics of wave disturbances in stable and unstable parallel flows—Part 2. The development of a solution for plane-Poiseuille flow and for plane-Couette flow, *J. Fluid Mech.* **9**, 371–389 (1960).
11. R. Mahadevan and G. M. Lilley, The stability of axial flow between concentric cylinders to asymmetric disturbances, *AGARD Conf. Proc.* No. 224, Paper No. 9 (1977).
12. W. C. Reynolds and M. C. Potter, Finite-amplitude instability of parallel shear flows, *J. Fluid Mech.* **27**, 465–492 (1967).

EFFET SUR LE TRANSFERT THERMIQUE DE L'INSTABILITE DE LA CONVECTION MIXTE DANS UN ESPACE ANNULAIRE VERTICAL

Résumé—On étudie la stabilité hydrodynamique de la convection mixte dans un espace annulaire. La limite de la stabilité linéaire est déterminée pour un écoulement ascendant dans un espace annulaire vertical avec application d'un flux thermique uniforme sur la paroi interne et isolation à l'extérieur. Le résultat indique que l'écoulement pleinement établi est thermiquement instable dans plusieurs régions d'un espace paramétrique approprié. Les valeurs des perturbations d'amplitude finie dans la région instable sont déterminées en utilisant l'hypothèse de forme de Stuart. On obtient des profils distordus d'écoulement moyen et les accroissements des transferts thermiques dûs à ces perturbations, calculés à partir des résultats, s'accordent bien avec les données expérimentales.

DER EINFLUSS VON GEMISCHTER KONVEKTION AUF DEN WÄRMEÜBERGANG IN EINEM VERTIKALEN RING

Zusammenfassung—Die hydrodynamische Stabilität bei Mischkonvektion in einem Ringspalt wird untersucht. Es wird die laminare Stabilitätsgrenze für eine erzwungene Aufwärtsströmung in einem vertikalen Ringspalt bestimmt, dessen innere Wand einem konstanten Wärmestrom ausgesetzt und dessen äußere Wand isoliert ist. Das Ergebnis zeigt, daß die voll entwickelte Strömung in den meisten Gebieten eines entsprechenden Parameterraumes thermisch instabil ist. Die Größe der Strörungen endlicher Amplitude in den instabilen Regionen werden über die Stuart'sche Formannahme bestimmt. Daraus ergeben sich gestörte mittlere Durchflußprofile. Der hierdurch hervorgerufene Anstieg des Wärmeübergangs wird aus den Ergebnissen berechnet und stimmt gut mit den experimentell ermittelten Daten überein.

ВЛИЯНИЕ НЕУСТОЙЧИВОСТИ ПРИ СМЕШАННОЙ КОНВЕКЦИИ НА ТЕПЛОПЕРЕНОС В ВЕРТИКАЛЬНО РАСПОЛОЖЕННОМ КОЛЬЦЕВОМ ЗАЗОРЕ

Аннотация—Исследуется гидродинамическая устойчивость смешанной конвекции в кольцевом зазоре. Определена граница линейной устойчивости восходящего вынужденного течения в вертикальном кольцевом зазоре, на внутренней стенке которого поддерживается постоянный тепловой поток, а внешняя теплоизолирована. Результаты показывают, что полностью развитое течение является термически неустойчивым в большей части области определяющих параметров. С использованием предположения Стюарта о форме определены значения конечных возмущений амплитуды в неустойчивой области. Получены возмущенные профили осредненного течения и по этим результатам рассчитано увеличение интенсивности теплопереноса, вызванное этими возумущениями. Расчеты хорошо согласуются с экспериментальными данными.